Synthesis, structure, and magnetic properties of the two-dimensional quantum antiferromagnets (CuBr)A(2)B(3)O(10) (A=Ca, Sr, Ba, Pb; B=Nb, Ta) with the 1/3 magnetization plateau

AUTHOR(S):

Tsujimoto, Y.; Kageyama, H.; Baba, Y.; Kitada, A.; Yamamoto, T.; Narumi, Y.; Kindo, K.; ... Ueda, Y.; Ajiro, Y.; Yoshimura, K.

CITATION:

Tsujimoto, Y. ...[et al]. Synthesis, structure, and magnetic properties of the two-dimensional quantum antiferromagnets (CuBr)A(2)B(3)O(10) (A=Ca, Sr, Ba, Pb; B=Nb, Ta) with the 1/3 magnetization plateau. PHYSICAL REVIEW B 2008, 78(21): 214410.

ISSUE DATE:

2008-12

URL:

http://hdl.handle.net/2433/109863

PHYSICAL REVIEW B **78**, 214410 (2008)

Synthesis, structure, and magnetic properties of the two-dimensional quantum antiferromagnets $(CuBr)A_2B_3O_{10}$ (A=Ca, Sr, Ba, Pb; B=Nb, Ta) with the 1/3 magnetization plateau

Y. Tsujimoto,[1] H. Kageyama,[1,*] Y. Baba,[1] A. Kitada,[1] T. Yamamoto,[1] Y. Narumi,[2] K. Kindo,[2] M. Nishi,[2] J. P. Carlo,[3] A. A. Aczel,[4] T. J. Williams,[4] T. Goko,[3,5] G. M. Luke,[4] Y. J. Uemura,[3] Y. Ueda,[2] Y. Ajiro,[1] and K. Yoshimura[1]

[1]*Department of Chemistry, Graduate School of Science, Kyoto University, Kyoto 606-8502, Japan*

[2]*Institute for Solid State Physics, University of Tokyo, Kashiwa, Chiba 277-8581, Japan*

[3]*Department of Physics, Columbia University, New York, New York 10027, USA*

[4]*Department of Physics and Astronomy, McMaster University, Hamilton, Ontario, Canada L8S 4M1*

[5]*TRIUMF, Vancouver, British Columbia, Canada V6T 2A3*

(Received 18 September 2008; revised manuscript received 28 October 2008; published 8 December 2008)

A 1/3 magnetization plateau was recently observed in the layered perovskite $(CuBr)Sr_2Nb_3O_{10}$ with $S=1/2$ CuBr layers. In order to control the cell size and thus exchange parameters, we have prepared an isostructural series of $(CuBr)A_2B_3O_{10}$ (A=Ca, Sr, Ba, Pb; B=Nb, Ta) and investigated the magnetic properties. We found that the stability of the 1/3 magnetization plateau is systematically tunable by the lattice parameter a. A substantial role played by the superexchange pathway via BO_6-BO_6 in the magnetic properties is suggested in addition to that via Br. Specific heat and muon spin relaxation measurements show that the appearance of the plateau phase is accompanied by successive phase transitions in low fields—the first one is possibly a structural transition and the second one is a magnetic transition. Frustration may induce the structural distortion and stabilize the 1/3 plateau phase.

DOI: 10.1103/PhysRevB.78.214410 PACS number(s): 75.45.+j, 72.80.Ga, 75.30.Et, 75.50.Ee

I. INTRODUCTION

Over the past several decades, geometrically frustrated antiferromagnets (AF) with small spins have attracted considerable attention in condensed-matter physics because of the emergence of novel quantum behaviors observed in most cases at low temperatures.[1,2] In particular, magnetic fields are a useful tool to drive transitions into interesting phases best featured by Bose-Einstein condensation (BEC) of magnons (triplets) and quantized magnetization plateaus.[3] Experimentally, a 1/2 plateau was obtained in $[Ni_2(Medpt)_2(\mu\text{-ox})(\mu\text{-}N_3)]ClO_4\cdot 0.5H_2O$ [Medpt=methyl-bis(3-aminopropyl) amine],[4] 1/3 plateau in the diamond chain $Cu_3(CO_3)_2(OH)_2$ (Ref. 5) and the Kagomé-lattice $Cu_3(titmb)_2(OCOCH_3)_6$ [titmb=1,3,5-tris(imidazol-1-ylmethyl)-2,4,6 trimethylbenzene],[6] 1/3 and 2/3 plateaus in the distorted triangular-lattice Cs_2CuBr_4,[7] and 1/8, 1/4, and 1/3 plateaus in the Shastry-Sutherland lattice $SrCu_2(BO_3)_2$.[8] All the observed plateaus seem to be in good agreement with Oshikawa *et al.*'s[9] theory which predicts a topological condition for the appearance of plateaus, $p(S-m)$=integer, where p and m are the period of the spin state and the magnetization per site, respectively.

We recently reported that a triple-layered perovskite $(CuBr)Sr_2Nb_3O_{10}$, obtained by an ion-exchange reaction, exhibits a quantized magnetization plateau at 1/3 of the fully saturated magnetization, and successive transitions in the low-field region (T_{c1}=9.3 K and T_{c2}=7.5 K at zero field).[10] As shown in Fig. 1, $(CuBr)Sr_2Nb_3O_{10}$ is of tetragonal symmetry and $CuBr_4$ squares edge share to form the $S=1/2$ layer, which is widely separated by nonmagnetic triple-layered perovskite blocks ($c\sim 16$ Å), making this compound a good two-dimensional quantum magnet. The observation of the 1/3 plateau is remarkable since it is naturally expected in triangle-based lattices. $(CuBr)Sr_2Nb_3O_{10}$ is characterized by the square-based lattice. For the simple J_1-J_2 model, where J_1 and J_2 denote nearest and next-nearest interactions, respectively, and plateaus such as 1/2 are expected.[11]

A big advantage for ion-exchange reactions is the rational preparation of desired structures, an ability that allows systematic tuning and understanding of the structural and physical properties. In the present case, the synthetic scheme to yield $(CuBr)Sr_2Nb_3O_{10}$ is generalized into $(CuX)A_{n-1}B_nO_{3n+1}$ (X=Cl, Br; A=La, Ca, Sr; B=Ti, Nb, Ta; n=2, 3). This versatility has been successfully demonstrated by magnetic studies of the double-layered (n=2) compounds ($c\sim 11$ Å), revealing a spin-singlet ground state and BEC of magnons in $(CuCl)LaNb_2O_7$,[12–14] collinear (stripe) magnetic order in $(CuBr)LaNb_2O_7$,[15] and quantum phase separation in $(CuCl)La(Nb_{1-x}Ta_x)_2O_7$.[16]

In this work, we have successfully synthesized a series of triple-layered copper bromides $(CuBr)A_2B_3O_{10}$ (A=Ca, Sr, Pb, Ba; B=Nb, Ta), and investigated the relation between structures and magnetic properties by means of x-ray diffraction (XRD), magnetic susceptibility, specific heat, high-field magnetization, and muon spin relaxation (μSR). Our main motivations are to understand how the 1/3 plateau phase as well as the low-field intermediate phase are influenced by the A- and B-site substitutions and obtain a general guide for searching compounds with magnetization plateaus.

II. EXPERIMENTAL PROCEDURES

A. Synthesis

For $A=(Ca_{1-x}Sr_x)$ (where x=0, 0.25, 0.5, 0.75, and 1), the parent compounds of the Dion-Jacobson-type layered perovskites $RbA_2B_3O_{10}$ (B=Nb, Ta) were synthesized by conventional high-temperature solid-state reactions as reported in the literature.[17] Starting reagents Rb_2CO_3 (>99.99%),

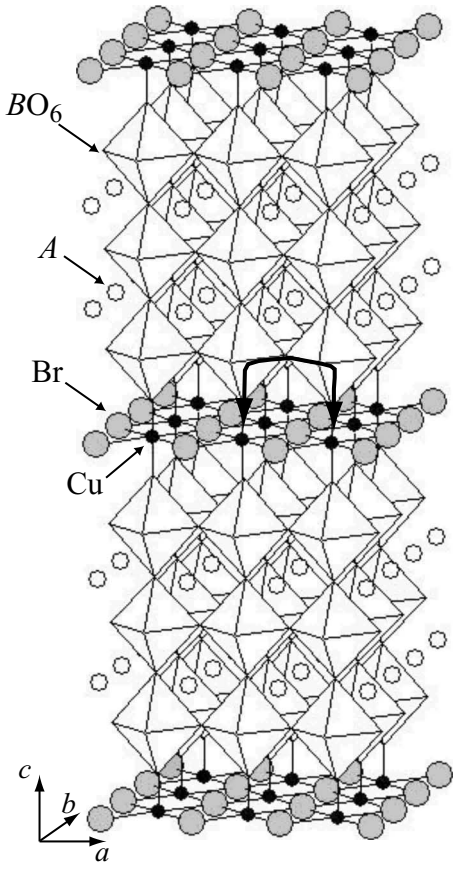

FIG. 1. Schematic crystal structure of (CuBr)$A_2B_3O_{10}$ (A=Ca, Sr, Ba, Pb; B=Nb, Ta). The arrow represents the superexchange path via BO_6-BO_6.

$CaCO_3$ (>99.99%), $SrCO_3$ (>99.99%), Nb_2O_5 (>99.999%), and Ta_2O_5 (>99.999%) were weighed in an appropriate stoichiometry for A and B and a 25% molar excess of Rb_2CO_3, and ground together with an agate mortar in an argon-filled glove box. Here, excess Rb_2CO_3 was added to compensate the loss due to its volatilization. Then the mixture was placed in an alumina crucible and heated in air under ambient pressure at 850 °C for 12 h. They were reground and heated to 1100 °C for 24 h. Subsequently, all the products were washed thoroughly with distilled water to remove the excess alkaline carbonate and dried overnight at 120 °C. Because the Rb compounds could not be formed for A=Pb and Ba,[18,19] Cs$A_2B_3O_{10}$ was prepared in a similar method as described above, using Cs_2CO_3 for A=Pb and $CsNO_3$ for A=Ba as starting reagent. $CsPb_2Nb_3O_{10}$ was prepared from stoichiometric quantities of PbO (>99.99%) and Nb_2O_5 with a 25% molar excess of Cs_2CO_3 (>99.99%), the mixture of which was heated at 850 °C for 12 h followed by additional heating at 1000 °C for 24 h with an intermediate grinding. Note that $CsPb_2Ta_3O_{10}$ could not be formed; instead of the desired phase, $Pb_3Ta_4O_{13}$ was found as a main phase together with a small amount of unidentified phases. The Ba compounds, $CsBa_2B_3O_{10}$ (B=Nb, Ta), were prepared from stoichiometric mixtures of $Ba(NO_3)_2$ (>99.99%) and B_2O_5 with a 25% molar excess of $CsNO_3$. The mixture was heated at 600 °C for 6 h and then at 850 °C for 3 h.

The syntheses of (CuBr)$A_2B_3O_{10}$ (A=Ca, Sr, Pb, Ba; B=Nb, Ta) were performed by low-temperature ion-exchange reactions between a corresponding parent phase and $CuBr_2$, as expressed by the following formula:

$$A'A_2B_3O_{10} + CuBr_2 \rightarrow (CuBr)A_2B_3O_{10} + A'Br$$

$$[A' = \text{Rb, Cs; } A = \text{(Ca, Sr), Ba, Pb; } B = \text{Nb, Ta}]. \quad (1)$$

Each parent compound was thoroughly ground with twofold molar excess of $CuBr_2$ (99.99%) in the argon-filled glove box and was hand pressed into a pellet. The pellet was transferred to a vacuum line without exposure to air, sealed in an evacuated Pyrex tube ($<10^{-3}$ Torr), and then heated for 7 days at 350 °C, the same temperature as employed to the synthesis of (CuBr)$LaNb_2O_7$.[15] The products were washed with distilled water to eliminate the byproduct (RbBr or CsBr) and unreacted $CuBr_2$, and dried overnight at 120 °C. All final products are insulating and brown in color such as (CuBr)$LaNb_2O_7$.

B. Characterizations

Powder XRD data of the samples before and after the ion-exchange reactions were typically collected between 2θ =5° and 80° with a step of 0.02° and a 0.1 s count time using a M18XHF diffractometer (Mac Science) with a graphite monochromator using Cu $K\alpha$ (λ=1.5418 Å) radiation. The impurity phases present in the products were identified using the standards from the JCPDS database with the help of the MXP software package equipped with the diffractometer. A step of 0.01° and a 2 s count time were employed to collect the data for the structural refinements. Rietveld refinements were performed using the RIETAN2000 program.[20] Profile refinements utilized the pseudo-Voigt function. The R factor (R_p), the weighted R factor (R_{wp}), and S are defined as the following profile: $R_p = \Sigma|y_{io} - y_{ic}|/\Sigma y_{io}$, weighting profile $R_{wp} = [\Sigma w_i(y_{io} - y_{ic})^2/\Sigma w_i y_{io}^2]$, and goodness of fit $S = R_{wp}/R_{exp}$. $R_{exp} = [(N-P)/\Sigma w_i y_{io}^2]^{1/2}$, where y_{io} and y_{ic} are the observed and calculated intensities, w_i is the weighting factor, N is the total number of y_{io} data when the background is refined, and P is the number of adjusted parameters.

Magnetic susceptibility measurements for (CuBr)$A_2B_3O_{10}$ were performed on a powder sample using a superconducting quantum interference device (SQUID) (Quantum Design, MPMS-XL-HKD) magnetometer over the temperature range T=2–300 K in an applied magnetic field of H=0.1 T in both field-cooled (FC) and zero-field-cooled (ZFC) processes. High-field magnetization measurements were made using an induction method with a multilayer pulse magnet installed at the Institute for Solid State Physics (ISSP) at the University of Tokyo. Magnetization data were collected at 4.2 and 1.3 K in magnetic fields of up to 60 T. Specific heat measurements were performed using a relaxation technique with a commercial physical property measurement system (PPMS) (Quantum Design) from 2 to 40 K in zero magnetic field. The hand-pressed pellet was mounted on an alumina plate with grease for better thermal contact. μSR measurements were carried out for (CuBr)$Sr_2Nb_3O_{10}$ and (CuBr)$Ba_2Ta_3O_{10}$ on the M20 surface muon beamline at TRIUMF. Spin-polarized positive muons were implanted in the powder samples in zero-field (ZF) μSR,[21] and the time

histograms of the forward-backward asymmetry of the decay positrons were recorded.

III. RESULTS

A. Synthesis and lattice parameters

The XRD patterns for all the parent compounds $A'A_2B_3O_{10}$ obtained in this study were readily indexed on the tetragonal cell with approximate lengths of 4 and 16 Å for the a and c axes, respectively. No trace of impurity phases was found in the profiles of the Ca-, Sr-, and Pb-based parent compounds within the experimental resolution of the present experimental conditions. On the other hand, the Ba-based parent compounds, $CsBa_2Nb_3O_{10}$ and $CsBa_2Ta_3O_{10}$, were yielded together with a small amount of nonmagnetic impurity $Ba_5Nb_4O_{15}$ (6%) and $Ba_5Ta_4O_{15}$ (4%), as also reported in the literature.[18] Here, the ratio of the main-to-impurity phase was roughly estimated from the relative intensity of XRD patterns. Attempts to yield pure phases by changing, e.g., reaction temperature and time did not improve the results.

The XRD patterns for $(CuBr)A_2B_3O_{10}$ were also indexable by the tetragonal symmetry without any extinction conditions. The lattice parameters are similar to those of reported compounds $(CuCl)Ca_2Nb_3O_{10}$ and $(CuCl)La_2Ti_2NbO_{10}$.[22] It is therefore natural to assume that the structures of all the ion-exchanged compounds obtained in the present study are identical with $(CuCl)Ca_2Nb_3O_{10}$ having the $P4/mmm$ space group. No impurity phase was found in $(CuBr)Ca_2Ta_3O_{10}$ and $(CuBr)Sr_2Ta_3O_{10}$ within experimental resolution. The Ba-based compounds were successfully formed but together with $Ba_5Nb_4O_{15}$ ($Ba_5Ta_4O_{15}$) which was already present after the high-temperature synthesis of $CsBa_2Nb_3O_{10}$ ($CsBa_2Ta_3O_{10}$). For the synthesis of $(CuBr)Pb_2Nb_3O_{10}$, PbO_2, to which $CsPb_2Nb_3O_{10}$ decomposed during the ion-exchange reaction, was yielded together with the main phase. These impurities could not be separated from the main product but the nonmagnetic nature of the impurity phases would not prevent us from capturing the essential magnetic features of $(CuBr)A_2B_3O_{10}$ at least from a qualitative point of view. Very weak unidentified peaks were detected in the XRD data of $(CuBr)Ca_2Nb_3O_{10}$, $(CuBr)Sr_2Nb_3O_{10}$, $(CuBr)Pb_2Nb_3O_{10}$, and $(CuBr)Ba_2B_3O_{10}$.

Figures 2(a) and 2(b) show the lattice parameters for $(CuBr)A_2B_3O_{10}$ (and corresponding precursors for comparison) plotted against the ionic radius of $r_{A^{2+}}$, where $r_{Ca^{2+}}=1.34$ Å, $r_{Sr^{2+}}=1.44$ Å, $r_{Pb^{2+}}=1.49$ Å, and $r_{Ba^{2+}}=1.61$ Å in the 12-fold coordination were used.[23] The lattice parameters were determined by least-squares calculations of selected peaks in the XRD profile. The average ionic radius of the solid solution between Sr and Ca is defined as that weighted for the relative molar ratio. It is recognized that the a lattice parameter slightly increases upon the ion-exchange reaction (1), which reflects the formation of a fairly rigid network consisting of corner-shared BO_6 octahedra. On the contrary, the expansion along the c axis relative to the parent compound is more prominent (0.7–0.8 Å), which is a consequence of the insertion of copper-bromine arrays in between

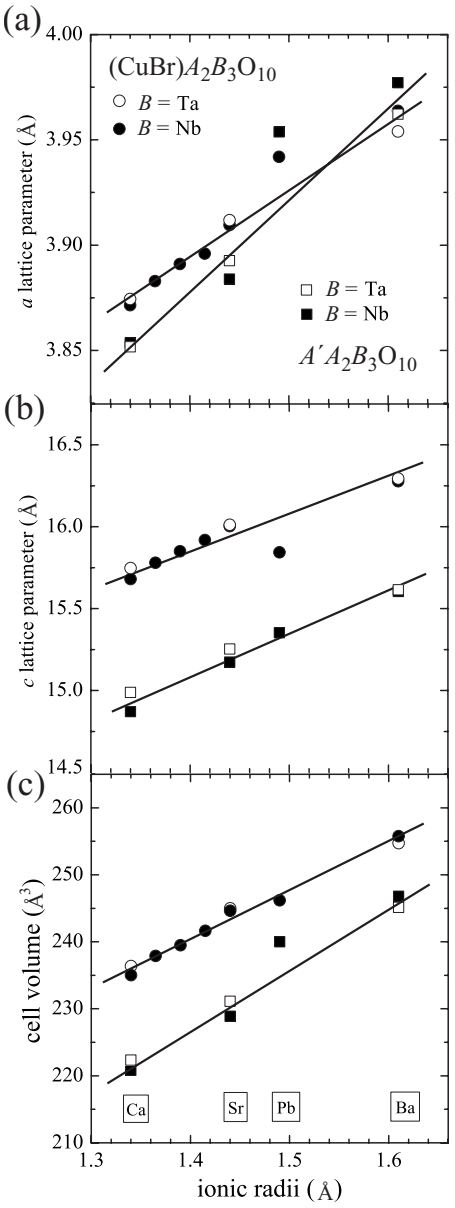

FIG. 2. Plots of the a and c lattice parameters and the cell volumes for (squares) $A'A_2B_3O_{10}$ (A'=Rb, Cs; A=Ca, Sr, Ba, Pb; B=Nb, Ta) and (circles) $(CuBr)A_2B_3O_{10}$.

perovskite blocks. The same trends have been observed in the known compounds.[22,24]

In the case of A=alkali earth metal, both cell parameters exhibit a linear increase with $r_{A^{2+}}$, as also observed for the parent compounds. In other words, both lattice parameters are insensitive to B. This observation is naturally understood considering the same ionic radius of ~0.64 Å for Nb^{5+} and Ta^{5+} in the sixfold coordination.[23] A notable feature has been observed when A is lead, i.e., $(CuBr)Pb_2Nb_3O_{10}$, where both lattice parameters show a slight deviation from the linear relation in Figs. 2(a) and 2(b) with the c lattice parameter being shorter than expected, whereas the a lattice parameter is longer. Note that a smaller difference in the c axis between daughter and mother compounds (~0.5 Å) for A=Pb would not be attributed to the incomplete ion-exchange reaction but to the steric effect of the $6s^2$ lone pair in Pb as observed in

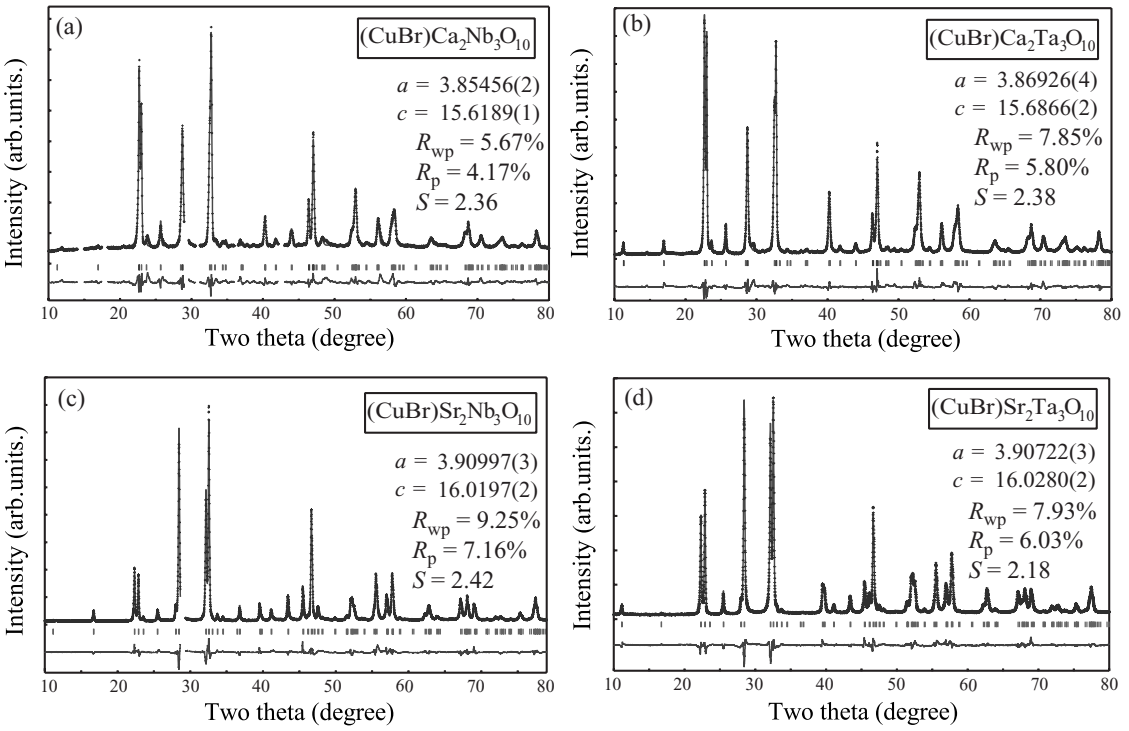

FIG. 3. Rietveld structure refinements for (a) $(CuBr)Ca_2Nb_3O_{10}$, (b) $(CuBr)Ca_2Ta_3O_{10}$, (c) $(CuBr)Sr_2Nb_3O_{10}$, and (d) $(CuBr)Sr_2Ta_3O_{10}$, showing the calculated (top, solid line) and observed (top, dotted line) XRD patterns. The difference is indicated by a solid line at the bottom. $(CuBr)A_2B_3O_{10}$ adapts to the space group $P4/mmm$ similar to $(CuCl)Ca_2Nb_3O_{10}$.

other oxides such as $PbVO_3$.[25] What is interesting in relation to this is that the cell volume of $(CuBr)A_2B_3O_{10}$ [Fig. 2(c)] exhibits linear behavior for the entire A site series including lead. The steric expansion in the cell volume of $CsPb_2Nb_3O_{10}$ originally induced by the lone pair in lead is likely released by the ion-exchange reaction.

Now we are in possession of compounds with variable lattice parameters governed by $r_{A^{2+}}$ (apart from a small deviation seen in A=Pb), allowing systematic investigation of the magnetism. Since the distance between the CuBr layers (i.e., the c lattice parameter) is much longer, the magnetic properties presented in Sec. III C would be mostly influenced by the a lattice parameter.

B. Structural refinements

The initial inspection of the XRD data of $(CuBr)A_2B_3O_{10}$ suggested that they adopt the same structure as $(CuCl)Ca_2Nb_3O_{10}$ with a tetragonal symmetry (space group $P4/mmm$).[22] Starting from this space group and atomic coordinates for $(CuCl)Ca_2Nb_3O_{10}$, we performed Rietveld refinement of the XRD profile of $(CuBr)Sr_2Nb_3O_{10}$. The isotropic displacement parameters U_{iso} of the oxygen and niobium atoms were independently constrained to the same value during refinement. The fit converged reasonably, providing R_{wp}=9.25% and R_p=7.16. The experimental and theoretical profiles and the difference are presented in Fig. 3(a). The refined structural parameters are shown in Table I. The fractional atomic positions do not differ largely from those of $(CuCl)Ca_2Nb_3O_{10}$. However, the U_{iso} for the bromine site, 0.097(2) Å^2, is extraordinarily large. This implies that the bromine ions in $(CuBr)Sr_2Nb_3O_{10}$ move off the 1d Wyckoff site $(\frac{1}{2}, \frac{1}{2}, \frac{1}{2})$, which was also proposed in the course of the refinement of $(CuX)LaB_2O_7$ (X=Cl, Br; B=Nb, Ta) and $(CuCl)Ca_2Nb_3O_{10}$.[22,24] Accordingly, the disorder model that placed the bromine on the 4m $(x, 0, \frac{1}{2})$ with a fixed site occupancy factor (sof) of 25% was examined, which resulted in x=0.439(3), and the U_{iso} for Br dropped to reasonable values [0.020(3)]. R factors R_{wp} and R_p were reduced to 9.15% and 7.07%. Refining the sof of the fourfold bromine site did not improve the results. We also tried to place bromine atoms at more general positions 8q $(x, y, \frac{1}{2})$ with a fixed sof of 0.125 but the fit ended up with $x \sim 0$.

Subsequently, we refined the crystal structures of $(CuBr)Ca_2Nb_3O_{10}$, $(CuBr)Ca_2Ta_3O_{10}$, and $(CuBr)Sr_2Ta_3O_{10}$ in the same way as $(CuBr)Sr_2Nb_3O_{10}$ but for simplicity without taking into account any disorder of the bromine atoms. The refinement converged reasonably, providing R_{wp} =5.21% and R_p=3.88 for $(CuBr)Ca_2Nb_3O_{10}$, R_{wp}=7.85% and R_p=5.80 for $(CuBr)Ca_2Ta_3O_{10}$, and R_{wp}=7.93% and R_p=6.03 for $(CuBr)Sr_2Ta_3O_{10}$. The profile fits and the structural parameters are represented in Figs. 3(b)–3(d) and Table I. As expected, the U_{iso} at the bromine site is large, suggesting the displacement of bromine atoms off the ideal position. The structures of the Ba- and Pb-containing compounds could not be refined because of the presence of the unidentified impurities.

C. Magnetic properties

1. Magnetic susceptibility

In Fig. 4, we present the temperature dependence of the magnetic susceptibilities χ ($\equiv M/H$) of $(CuBr)A_2B_3O_{10}$ [A

TABLE I. The crystallographic data for $(CuBr)A_2B_3O_{10}$ (A=Ca, Sr; B=Nb, Ta).

Atom	Site	x	y	z	g [a]	$100U_{iso}$ (Å^2)[b]
(A,B)=(Ca,Nb)						
Cu	1b	0	0	0.5	1.00(2)	4.0(3)
Br	1d	0.5	0.5	0.5	1.05(2)	7.8(4)
Ca	2h	0.5	0.5	0.1431(3)	1	1.27(17)
Nb1	1a	0	0	0	1	0.5(1)
Nb2	2g	0	0	0.2668(1)	1	0.5
O1	2f	0	0.5	0	1	4.0(2)
O2	2g	0	0	0.122(1)	1	4
O3	4i	0	0.5	0.2441(9)	1	4
O4	2g	0	0	0.365(1)	1	4
(A,B)=(Ca,Ta)						
Cu	1b	0	0	0.5	1.011(8)	2.3(2)
Br	1d	0.5	0.5	0.5	1.049(7)	9.7(2)
Ca	2h	0.5	0.5	0.1427(2)	1	0.86(12)
Ta1	1a	0	0	0	1	0.058(14)
Ta2	2g	0	0	0.269 69(7)	1	0.05
O1	2f	0	0.5	0	1	3.98(17)
O2	2g	0	0	0.1213(8)	1	3.9
O3	4i	0	0.5	0.2444(6)	1	3.9
O4	2g	0	0	0.3739(9)	1	3.9
(A,B)=(Sr,Nb)						
Cu	1b	0	0	0.5	0.959(7)	1.7(2)
Br	1d	0.5	0.5	0.5	0.976(6)	4.41(19)
Sr	2h	0.5	0.5	0.1389(1)	1	0.84(5)
Nb1	1a	0	0	0	1	0.04(3)
Nb2	2g	0	0	0.272 77(9)	1	0.04
O1	2f	0	0.5	0	1	1.19(13)
O2	2g	0	0	0.1218(5)	1	1.1
O3	4i	0	0.5	0.2481(3)	1	1.1
O4	2g	0	0	0.3807(6)	1	1.1
(A,B)=(Sr,Ta)						
Cu	1b	0	0	0.5	0.948(9)	0.8(2)
Br	1d	0.5	0.5	0.5	1.048(7)	5.8(2)
Sr	2h	0.5	0.5	0.139 30(13)	1	0.12(6)
Ta1	1a	0	0	0	1	0.55(2)
Ta2	2g	0	0	0.27284(7)	1	0.55
O1	2f	0	0.5	0	1	0.30(14)
O2	2g	0	0	0.1252(7)	1	0.3
O3	4i	0	0.5	0.2462(5)	1	0.3
O4	2g	0	0	0.3900(7)	1	0.3

[a]g is the site occupancy.
[b]The isotropic displacement parameters U_{iso} of oxygen, niobium, and tantalum are independently constrained to the same values while in the refinement.

=Ca (Fig. 4(a)), Sr (Fig. 4(b)), Pb (Fig.4(c)), and Ba (Fig. 4(d))] measured in zero-field cooling mode. No differences are seen between ZF and field coolings. The reciprocal susceptibilities exhibit concave curves in the high-temperature region, pointing to a sizable contribution of diamagnetism from core electrons and/or aforementioned nonmagnetic impurities. Thus, fitting to the Curie-Weiss law plus a T-independent term, $\chi(T)=C/(T-\theta)+\chi_0$, where C and θ represent the Curie constant and the Weiss temperature, respectively, was performed in the temperature range T =100–300 K. The obtained parameters are listed in Table II. The values of C agree well with that expected for 1 mol of

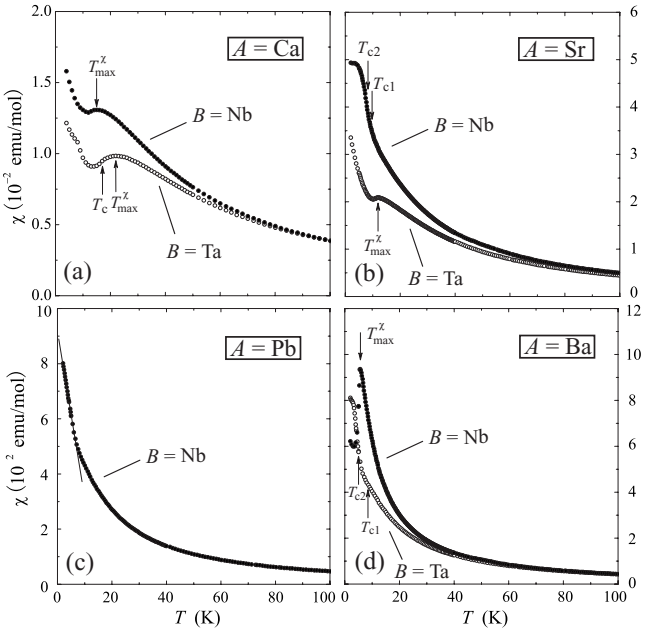

FIG. 4. The magnetic susceptibilities of (CuBr)$A_2B_3O_{10}$ measured in a field of 0.1 T after cooling in zero field.

Cu^{2+} ions (0.375 emu K/mol) and $g=2$, supporting the designated compositions. Common to the (CuBr)$A_2B_3O_{10}$ family, θ is positive, indicating that the ferromagnetic (FM) interaction is dominant in contrast to the double-layered system (CuX)$LaNb_2O_7$ (X=Cl, Br) having negative θ. From the A site dependence of the a lattice parameter in (CuBr)$A_2B_3O_{10}$, it is intuitively expected that θ changes linearly as a function of $r_{A^{2+}}$. In practice, however, θ depends on both A- and B-site ions despite the structural closeness between Nb and Ta compounds for a given A. This may indicate complex superexchange pathways as will be discussed later.

The χ-T curves of the A=Ca case, (CuBr)$Ca_2Nb_3O_{10}$ and (CuBr)$Ca_2Ta_3O_{10}$, exhibit a broad maximum, a characteristic behavior of low-dimensional quantum antiferromagnets, but the temperature at which χ takes a maximum value, $T^{\chi}_{\max}$, differs between Nb ($T^{\chi}_{\max}$=15 K) and Ta ($T^{\chi}_{\max}$=22 K). A Curie tail at lower temperatures would be due to a small amount of defects in the CuBr layer and/or residual impurities. For A=Sr, the χ of (CuBr)$Sr_2Ta_3O_{10}$ ($T^{\chi}_{\max}$=12 K) is similar to those of the Ca systems. By marked contrast, (CuBr)$Sr_2Nb_3O_{10}$ apparently has a featureless curve with a monotonic increase and finally flattens out at lower temperatures. Our previous specific-heat experiments, however, revealed successive phase transitions at 9.3 K ($=T_{c1}$) and 7.5 K ($=T_{c2}$), which was discussed in terms of the competition (or frustration) between mixed (FM- and AF-) interactions in the CuBr layer.[10] For A=Pb, the χ-T curve increases monotonically with decreasing temperatures but a kink implying a magnetic transition was observed at around 6 K. For A=Ba, (CuBr)$Ba_2Nb_3O_{10}$ shows a drastic drop at 5 K, suggesting an antiferromagnetic transition, while (CuBr)$Ba_2Ta_3O_{10}$ shows a featureless temperature dependence similar to that of (CuBr)$Sr_2Nb_3O_{10}$.

TABLE II. The parameters obtained by Curie-Weiss fit to the susceptibilities of (CuBr)$A_2B_3O_{10}$. C, θ, and χ_0 represent Curie constant, Weiss temperature, and T-independent term, respectively.

Compound	C (emu K/mol)	θ (K)	$\chi_0\times10^4$ (emu/mol)
(CuBr)$Ca_2Nb_3O_{10}$	0.3985(6)	4.6(1)	−3.08(1)
(CuBr)$Ca_2Ta_3O_{10}$	0.383(1)	3.2(2)	−0.71(2)
(CuBr)$Sr_2Nb_3O_{10}$	0.408(1)	20.9(3)	−1.36(3)
(CuBr)$Sr_2Ta_3O_{10}$	0.423(2)	13.2(4)	−3.85(5)
(CuBr)$Ba_2Nb_3O_{10}$	0.399(2)	14.9(6)	−4.79(6)
(CuBr)$Ba_2Ta_3O_{10}$	0.404(1)	14.7(3)	−4.21(3)
(CuBr)$Pb_2Nb_3O_{10}$	0.4366(9)	17.4(2)	−5.27(2)

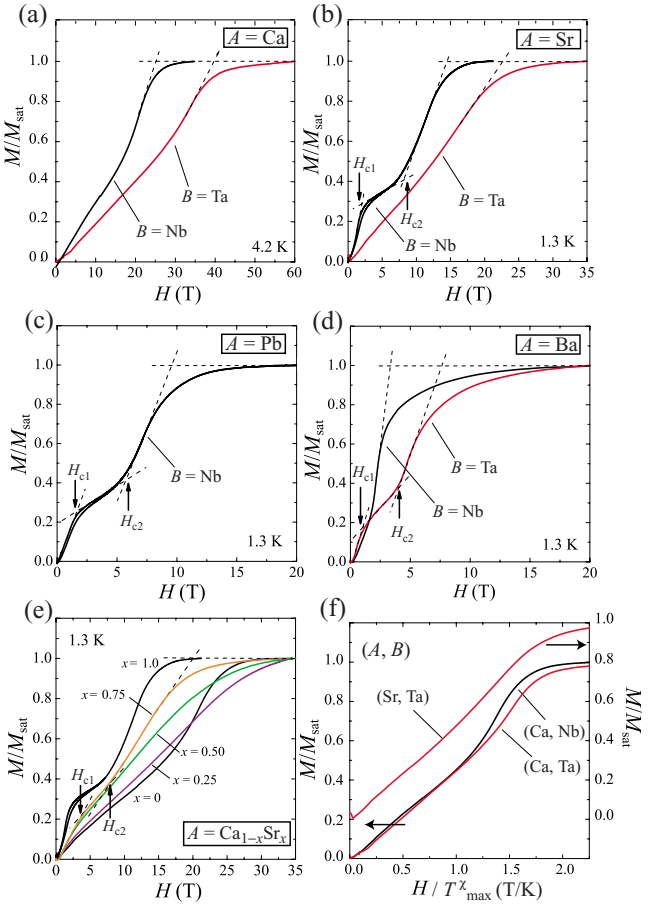

FIG. 5. (Color online) (a)-(e) Magnetization curves measured at 1.3 or 4.2 K for (CuBr)$A_2B_3O_{10}$. (f) Magnetization curves of (CuBr)$Ca_2B_3O_{10}$ and (CuBr)$Sr_2Ta_3O_{10}$ scaled by the temperature of the maximum susceptibility $T^{\chi}_{\max}$. For clarity, the magnetization of (CuBr)$Sr_2Ta_3O_{10}$ is shifted by 0.2.

2. *Magnetization curves*

Figure 5 depicts the magnetizations $M(H)$ of (CuBr)$A_2B_3O_{10}$ [A=Ca (Fig. 5(a)), Sr (Fig. 5(b)), Pb (Fig. 5(c)), and Ba (Fig. 5(d))] normalized by the saturation magnetizations M_s at 1.3 or 4.2 K. Let us first discuss the results of the B=Nb system. As previously reported,[10] (CuBr)$Sr_2Nb_3O_{10}$ exhibits a 1/3 magnetization plateau be-

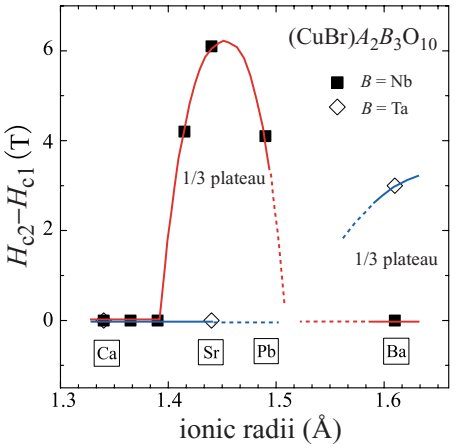

FIG. 6. (Color online) The compositional dependence of the plateau width $H_{c2}-H_{c1}$ in (CuBr)$A_2B_3O_{10}$ as a function of the ionic radius of the A site. The lines are drawn as guides for the eyes.

tween 2.0 T (=H_{c1}) and 8.1 T (=H_{c2}), and there is a small hysteresis below 3 T. Substitution chemistry revealed that the 1/3 plateau is indeed robust. As seen in Fig. 5(c), the magnetization of (CuBr)$Pb_2Nb_3O_{10}$ also exhibits a 1/3 plateau between H_{c1}=1.7 T and H_{c2}=5.8 T along with a small hysteresis below 2.5 T. The width of the plateau, $H_{c2}-H_{c1}$, is 4.1 T, which is narrower than 6.1 T in (CuBr)$Sr_2Nb_3O_{10}$, indicating that the A-site replacement by the larger cation destabilizes the plateau phase. Further increasing of the size of the A-site cation leads to the disappearance of the plateau; no plateau was observed in (CuBr)$Ba_2Nb_3O_{10}$ [Fig. 5(d)]. Decreasing the size of the A site (vs Sr) also results in the same outcome; no plateau was observed in (CuBr)$Ca_2Nb_3O_{10}$ [Fig. 5(a)]. Instead, the magnetization increases linearly in the low-field region, followed by nonlinear growth until it saturates. The nonlinear growth is possibly associated with quantum effects as reported for the double-layered system (CuBr)$LaNb_2O_7$.[15] Magnetization measurements were also conducted for the solid solution (CuBr)$(Ca_{1-x}Sr_x)_2Nb_3O_{10}$ (x=0.25, 0.50, and 0.75), as shown in Fig. 5(e). We observed a 1/3 plateau only for x=0.75. As shown in Fig. 6, the $H_{c2}-H_{c1}$ vs $r_{A^{2+}}$ plot clearly demonstrates an intimate correlation between $r_{A^{2+}}$ (or more specifically, the a lattice parameter) and the stability of the plateau phase.

The 1/3 plateau phase can be tuned not only by the A site but also by the B site. In the case of B=Ta, only (CuBr)$Ba_2Ta_3O_{10}$ showed a 1/3 plateau (H_{c1}=1.0 T and H_{c2}=4.0 T). It is interesting that there exists a converse relation: no plateau for (A,B)=(Sr, Ta) and (Ba, Nb), and plateaus for (Ba, Ta) and (Sr, Nb). Although the data available are limited, it is anticipated that, in analogy to the Nb case, the plateau-stabilizing region is shifted to the right in Fig. 6. Conditions for the appearance of the plateau would come from a subtle balance between the magnetic interactions mediated by Br and those mediated by BO_6-BO_6 (see Fig. 1).

3. Heat capacity

Figure 7 shows the temperature dependence of the total heat capacity C_p in zero magnetic field for

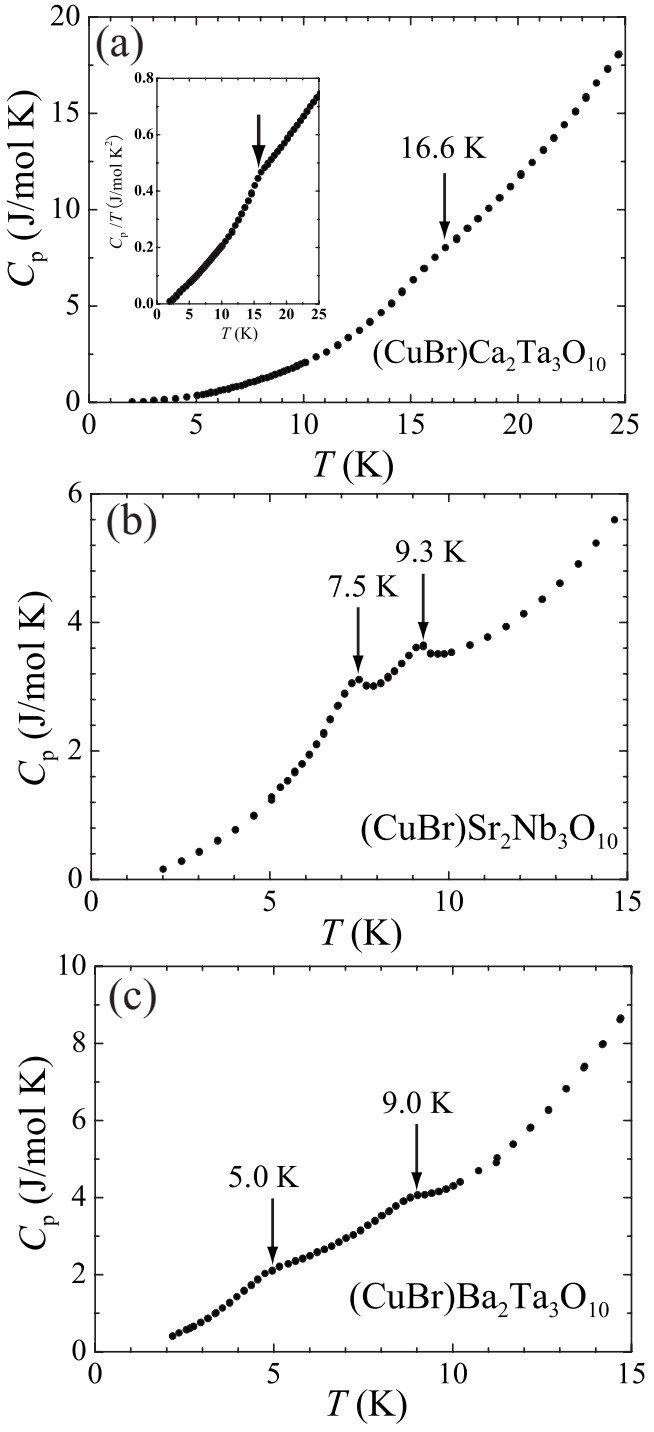

FIG. 7. The temperature variation in the heat capacity on (CuBr)$Ca_2Ta_3O_{10}$, (CuBr)$Sr_2Nb_3O_{10}$, and (CuBr)$Ba_2Ta_3O_{10}$. The C_p/T is shown in the inset to emphasize the anomaly at the transition temperature.

(CuBr)$Ca_2Ta_3O_{10}$, (CuBr)$Sr_2Nb_3O_{10}$, and (CuBr)$Ba_2Ta_3O_{10}$. (CuBr)$Ca_2Ta_3O_{10}$ exhibits a tiny anomaly at 16.6 K. This temperature is slightly below T^{χ}_{max} so that it is attributed to the onset of long-range magnetic order. As reported previously,[10] (CuBr)$Sr_2Nb_3O_{10}$ undergoes successive second-order-like phase transitions at T_{c1}=9.3 K and T_{c2}=7.5 K. Interestingly, (CuBr)$Ba_2Ta_3O_{10}$ undergoes succes-

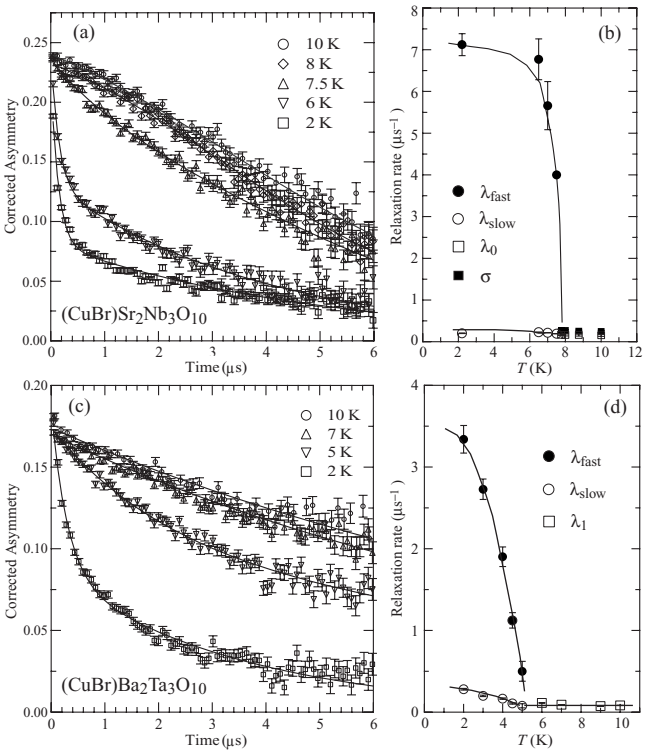

FIG. 8. (a),(c) The time evolution of μSR asymmetry and (b),(d) the temperature dependence of estimated relaxation rate in zero field for $(CuBr)Sr_2Nb_3O_{10}$ and $(CuBr)Ba_2Ta_3O_{10}$. The solid lines are guides for the eyes.

sive phase transitions as well at $T_{c1}=9.0$ K and $T_{c2}=5.0$ K. Therefore, successive phase transitions should be common to materials with a 1/3 plateau in their magnetizations.

4. Muon spin relaxation

To obtain more insight into the nature of successive phase transitions observed in $(CuBr)Sr_2Nb_3O_{10}$ and $(CuBr)Ba_2Ta_3O_{10}$, we have performed μSR measurements, which offer a unique opportunity in detecting a static magnetic order at high sensitivity. Figure 8(a) shows the temperature-dependent ZF-μSR spectra for $(CuBr)Sr_2Nb_3O_{10}$. At high temperatures above T_{c1}, the corrected asymmetry $A(t)$ shows a Gaussian-like decay, in consistency with a paramagnetic state. However, such a Gaussian-like decay continues even below T_{c1}, meaning that the intermediate state for $T_{c2}<T<T_{c1}$ is paramagnetic, in disagreement with the previous interpretation that the transition at T_{c1} is magnetic in nature.[10] The spectrum shape changes drastically from Gaussian to exponential below T_{c2}, confirming that long-range magnetic order onsets at T_{c2}.

The time spectra above T_{c2} were best fitted by the following formula:

$$A(t)=A_1\exp[-(\sigma t)^2]+A_2\exp(-\lambda_0 t). \quad (2)$$

The first term is the Kubo-Toyabe function that describes nuclear dipole relaxations. The second term takes into consideration the development of two-dimensional magnetic correlations among $S=1/2$ spins of Cu^{2+}, providing a dynamical field. $A_{1,2}$ are the fractional site population of the muons. The μSR spectra below T_{c2} were analyzed using the sum of two exponential functions,

$$A(t)=A_3\exp(-\lambda_{fast}t)+A_4\exp(-\lambda_{slow}t). \quad (3)$$

The calculated relaxation rates are given in Fig. 8(b). They rapidly increase at T_{c2} and saturate toward $T\rightarrow 0$. The two components of the relaxation rates may originate either from two crystallographically inequivalent muon sites or from a structurally unique but magnetically inequivalent site.

Figure 8(c) shows the ZF-μSR spectra for $(CuBr)Ba_2Ta_3O_{10}$. The spectra exhibit, like $(CuBr)Sr_2Nb_3O_{10}$, slow relaxation for $T>T_{c2}$ and fast relaxation for $T<T_{c2}$. The damping of the $A(t)$ becomes faster below 5 K ($=T_{c2}$) owing to the slowing down of fluctuations of Cu^{2+} spins. This demonstrates that the successive phase transitions derive from the same mechanism, whatever it is. Unlike $(CuBr)Sr_2Nb_3O_{10}$, however, $A(t)$ above T_{c2} could be fitted by a single exponential equation with relaxation rate λ_1 while the relaxation rate below T_{c2} was obtained by fitting the asymmetry curves to Eq. (3). Similar behavior was found in the paramagnetic state of a quasi-one-dimensional chain $Ca_3Co_2O_6$.[26,27]

IV. DISCUSSION

In the early stages of the magnetic study on these ion-exchanged materials, it was simply assumed that the perovskite blocks $A_{n-1}B_nO_{3n+1}$ were magnetically inert and that only the superexchange pathway through Cu-*X*-Cu determined the magnetic properties.[12] However, the susceptibilities and magnetizations in the present study show *B*-dependent behavior, indicating that in-plane superexchange interactions of Cu-BO_6-BO_6-Cu provide a significant contribution, in addition to those of Cu-Br-Cu. In general, one takes it for granted that the superexchange interaction through a nonmagnetic polyhedron such as SO_4, PO_4, and BO_3 is negligibly small in comparison with that through a single anion such as O, Cl, and Br, yet the former becomes in some cases dominant over the latter. A representative example is found in $(VO)_2P_2O_7$, which was once thought as a spin ladder system from the naive argument of the chemical structure[28,29] but then turned out to be a one-dimensional alternating chain system with the strongest exchange given by the V-PO_4-V pathway.[30] From the NMR study of $(CuCl)LaNb_2O_7$, the d_{z^2} orbital along the *c* axis (thus pointing to the neighboring BO_6 octahedra) is assigned as the orbital to accommodate an unpaired electron.[31] It is highly possible that $(CuBr)A_2B_3O_{10}$ employs the same electronic configurations which facilitate the hybridization between d_{z^2} orbitals and BO_6 octahedra.[32]

How are the magnetic interactions of $(CuBr)A_2B_3O_{10}$ affected by chemical substitution? $(CuBr)Ca_2Nb_3O_{10}$, $(CuBr)Ca_2Ta_3O_{10}$, and $(CuBr)Sr_2Ta_3O_{10}$ show a broad maximum in the susceptibility at $T^{\chi}_{max}=15$, 22, and 12 K, respectively. In accordance with T^{χ}_{max}, the saturation magnetic field changes: $H_s=25.1$, 39.8, and 22.7 T. As shown in Fig. 5(f), the magnetization curves are scaled by T^{χ}_{max}, demonstrating that the magnitude of the magnetic interactions is tuned by

the A-site as well as B-site substitutions. Comparison between $(CuBr)Ca_2Ta_3O_{10}$ and $(CuBr)Sr_2Ta_3O_{10}$ suggests that magnetic interactions become stronger by decreasing the a lattice parameter. However, the situation is not so simple since the appearance condition of the 1/3 plateau should be linked to the ratio of magnetic interactions. The implication of the domelike structure of the plateau width (Fig. 6) is that the a lattice parameter influences not only the magnitude but also the relative ratio. Here, we wish to recall that $(CuBr)Sr_2Nb_3O_{10}$ with the largest $\theta\,(>0)$ showed the widest plateau. Thus, increased ferromagnetic interactions (vs antiferromagnetic interaction) will result in stabilizing the 1/3 plateau phase.

It would be difficult to explain the experimentally observed 1/3 plateau in the framework of the J_1-J_2 model. Recently, Shannon and Momoi[33] theoretically investigated the J_1-J_2-J_3 model and showed the 1/3 plateau in a certain parameter range. However, we would like to stress the fact that the 1/3 plateau in the high-field magnetization curve is accompanied by successive phase transitions at low field. Applying the quantization condition $p(S-m)=$integer ($S=1/2$, $m=1/6$) to the present case, one obtains $p=3$ (or 6, 9,…). Therefore, the structural transition at T_{c1} involves a breaking of the translational symmetry that triples the unit cell of the crystal structure. In relation to this, the coupled dimer system NH_4CuCl_3 shows a structural phase transition involving a doubling of the unit cell in zero field, which is crucial for the appearance of the 1/4 and 3/4 magnetization plateaus.[34] It would be possible in our compounds that the structural transition at T_{c1} triggers the 1/3 plateau: it may change the symmetry and make some magnetic interactions nonequivalent. Further structural studies at low temperatures, in particular, synchrotron XRD and TEM, are highly desired. Single-crystal growth is also in progress.

V. CONCLUSIONS

We have synthesized a series of layered compounds containing two-dimensional CuBr layers by ion-exchange reactions with $CuBr_2$ of $A'A_2B_3O_{10}$ (A'=Rb, Cs; A=Ca, Sr, Ba, Pb; B=Nb, Ta). The Rietveld refinements for the powder XRD patterns have revealed that $(CuBr)A_2B_3O_{10}$ (A=Ca, Sr; B=Nb, Ta) are isostructural with $(CuCl)Ca_2Nb_3O_{10}$ with the space group of $P4/mmm$ although rather large thermal parameters of the bromine ion suggest statistically disordered distribution into more general sites. The lattice parameters predominantly change with the size of the A site ion, apart from a small deviation for A=Pb. The stability of the 1/3 magnetization plateau is controlled systematically by the a lattice parameter. Furthermore, the successive phase transitions were observed at zero field and assigned as the structural one at T_{c1} and the magnetic one at T_{c2}. It is considered that the former is derived from the rearrangement in the CuBr layer, leading to stabilization of the 1/3 plateau phase in high fields. Further experimental efforts and theoretical support are needed for full understanding of the relation between the structural and magnetic properties in $(CuBr)A_2B_3O_{10}$.

ACKNOWLEDGMENTS

This work was supported by Grants-in-Aid for Science Research on Priority Areas "Novel States of Matter Induced by Frustration" (No. 19052004) and "Invention of Anomalous Quantum Materials" (No. 16076210) from the Ministry of Education, Culture, Sports, Science and Technology of Japan, and by the Global COE program International Center for Integrated Research and Advanced Education in Material Science, Kyoto University, Japan. The μSR work was supported by JSPS and NSF under the Japan-U.S. Cooperative Science Program "Phase separation near quantum critical point in low-dimensional quantum spin systems" (Contract No. 14508500001). The work at Columbia University was supported by U.S. NSF Grants No. DMR-05-02706 and No. DMR-08-06846.

*Author to whom correspondence should be addressed; kage@kuchem.kyoto-u.ac.jp

[1] A. P. Ramirez, Annu. Rev. Mater. Sci. **24**, 453 (1994).
[2] M. F. Collins and O. A. Petrenko, Can. J. Phys. **75**, 605 (1997).
[3] T. M. Rice, Science **298**, 760 (2002).
[4] Y. Narumi, M. Hagiwara, R. Sato, K. Kindo, H. Nakano, and M. Takahashi, Physica B **246-247**, 509 (1998).
[5] H. Kikuchi, Y. Fujii, M. Chiba, S. Mitsudo, T. Idehara, T. Tonegawa, K. Okamoto, T. Sakai, T. Kuwai, and H. Ohta, Phys. Rev. Lett. **94**, 227201 (2005).
[6] Y. Narumi, K. Katsumata, Z. Honda, J. C. Domenge, P. Sindzingre, C. Lhuillier, Y. Shimaoka, T. C. Kobayashi, and K. Kindo, Europhys. Lett. **65**, 705 (2004).
[7] T. Ono, H. Tanaka, O. Kolomiyets, H. Mitamura, T. Goto, K. Nakajima, A. Oosawa, Y. Koike, K. Kakurai, J. Klenke, P. Smeibidle, and M. Meißner, J. Phys.: Condens. Matter **16**, S773 (2004).
[8] K. Onizuka, H. Kageyama, Y. Narumi, K. Kindo, Y. Ueda, and T. Goto J. Phys. Soc. Jpn. **69**, 1016 (2000).
[9] M. Oshikawa, M. Yamanaka, and I. Affleck, Phys. Rev. Lett. **78**, 1984 (1997).
[10] Y. Tsujimoto, Y. Baba, N. Oba, H. Kageyama, T. Fukui, Y. Narumi, K. Kindo, T. Saito, M. Takano, Y. Ajiro, and K. Yoshimura, J. Phys. Soc. Jpn. **76**, 063711 (2007).
[11] A. Honecker, Can. J. Phys. **79**, 1557 (2001).
[12] H. Kageyama, T. Kitano, N. Oba, M. Nishi, S. Nagai, K. Hirota, L. Viciu, J. B. Wiley, J. Yasuda, Y. Baba, Y. Ajiro, and K. Yoshimura, J. Phys. Soc. Jpn. **74**, 1702 (2005).
[13] H. Kageyama, J. Yasuda, T. Kitano, K. Totsuka, Y. Narumi, M. Hagiwara, K. Kindo, Y. Baba, N. Oba, Y. Ajiro, and K. Yoshimura, J. Phys. Soc. Jpn. **74**, 1702 (2005).
[14] A. Kitada, Z. Hiroi, Y. Tsujimoto, T. Kitano, H. Kageyama, Y. Ajiro, and K. Yoshimura, J. Phys. Soc. Jpn. **76**, 093706 (2007).
[15] N. Oba, H. Kageyama, T. Kitano, J. Yasuda, Y. Baba, M. Nishi, K. Hirota, Y. Narumi, M. Hagiwara, K. Kindo, T. Saito, Y. Ajiro, and K. Yoshimura, J. Phys. Soc. Jpn. **75**, 113601 (2006).

[16] Y. J. Uemura, A. A. Aczel, Y. Ajiro, J. P. Carlo, T. Goko, D. A. Goldfeld, A. Kitada, G. M. Luke, G. J. MacDougall, I. G. Mihailescu, J. A. Rodriguez, P. L. Russo, Y. Tsujimoto, C. R. Wiebe, T. J. Williams, K. Yoshimura, and H. Kageyama, arXiv:0806.2021 (unpublished).
[17] H. Kageyama, T. Kitano, R. Nakanishi, J. Yasuda, N. Oba, Y. Baba, M. Nishi, Y. Ueda, Y. Ajiro, and K. Yoshimura, Prog. Theor. Phys. Suppl. **159**, (Suppl.), 39 (2005).
[18] V. Thangadurai, P. S. Beurmann, and W. Weppner, J. Solid State Chem. **158**, 279 (2001).
[19] M. A. Subramanian, J. Goparakrishnan, and A. W. Sleight, Mater. Res. Bull. **23**, 837 (1988).
[20] F. Izumi and T. Ikeda, Mater. Sci. Forum. **198**, 321 (2000).
[21] R. S. Hayano, Y. J. Uemura, J. Imazato, N. Nishida, T. Yamazaki, and R. Kubo, Phys. Rev. B **20**, 850 (1979).
[22] T. A. Kodenkandath, A. S. Kumbhar, W. L. Zhou, and J. B. Wiley, Inorg. Chem. **40**, 710 (2001).
[23] R. D. Shannon, Acta Crystallogr. A **32**, 751 (1976).
[24] T. A. Kodenkandath, J. N. Lalena, W. L. Zhou, E. E. Carpenter, C. Sangregorio, A. U. Falster, W. B. Simmons, Jr., C. J. O'Connor, and J. B. Wiley, J. Am. Chem. Soc. **121**, 10743 (1999).
[25] A. A. Belik, M. Azuma, T. Saito, Y. Shimakawa, and M. Takano, Chem. Mater. **17**, 269 (2005).
[26] J. Sugiyama, H. Nozaki, J. H. Brewer, E. J. Ansaldo, T. Takami, H. Ikuta, and U. Mizutani, Phys. Rev. B **72**, 064418 (2005).
[27] S. Takeshita, J. Arai, T. Goko, K. Nishiyama, and K. Nagamine, J. Phys. Soc. Jpn. **75**, 034712 (2006).
[28] D. C. Johnston, J. W. Johnson, D. P. Goshorn, and A. J. Jacobson, Phys. Rev. B **35**, 219 (1987).
[29] T. Barnes and J. Riera, Phys. Rev. B **50**, 6817 (1994).
[30] A. W. Garrett, S. E. Nagler, D. A. Tennant, B. C. Sales, and T. Barnes, Phys. Rev. Lett. **79**, 745 (1997).
[31] M. Yoshida, N. Ogata, M. Takigawa, J. Yamaura, M. Ichihara, T. Kitano, H. Kageyama, Y. Ajiro, and K. Yoshimura, J. Phys. Soc. Jpn. **76**, 104703 (2007).
[32] M. Yoshida, N. Ogata, M. Takigawa, J. Yamaura, M. Ichihara, T. Kitano, H. Kageyama, Y. Ajiro, and K. Yoshimura, J. Phys. Soc. Jpn. **77**, 104705 (2008).
[33] N. Shannon and T. Momoi (private communication).
[34] Ch. Rüegg, M. Oettli, J. Schefer, O. Zaharko, A. Furrer, H. Tanaka, K. W. Krämer, H.-U. Güdel, P. Vorderwisch, K. Habicht, T. Polinski, and M. Meissner, Phys. Rev. Lett. **93**, 037207 (2004).